

Active RIS vs. Passive RIS: Which Will Prevail in 6G?

Zijian Zhang, Linglong Dai, *Fellow, IEEE*, Xibi Chen, Changhao Liu, Fan Yang, *Fellow, IEEE*, Robert Schober, *Fellow, IEEE*, and H. Vincent Poor, *Life Fellow, IEEE*

Abstract—As a revolutionary paradigm for controlling wireless channels, reconfigurable intelligent surfaces (RISs) have emerged as a candidate technology for future 6G networks. However, due to the “multiplicative fading” effect, the existing passive RISs only achieve a negligible capacity gain in many scenarios with strong direct links. In this paper, the concept of active RISs is proposed to overcome this fundamental limitation. Unlike the existing passive RISs that reflect signals without amplification, active RISs can amplify the reflected signals via amplifiers integrated into their elements. To characterize the signal amplification and incorporate the noise introduced by the active components, we develop a signal model for active RISs, which is validated through experimental measurements on a fabricated active RIS element. Based on the developed signal model, we further analyze the asymptotic performance of active RISs to reveal the substantial capacity gain they provide for wireless communications. Finally, we formulate the sum-rate maximization problem for an active RIS aided multiple-input multiple-output (MIMO) system and a joint transmit beamforming and reflect precoding algorithm is proposed to solve this problem. Simulation results show that, in a typical wireless system, the existing passive RISs can realize only a negligible sum-rate gain of 3%, while the proposed active RISs can achieve a significant sum-rate gain of 67%, thus overcoming the “multiplicative fading” effect.

Index Terms—Reconfigurable intelligent surface (RIS), beamforming, active RIS, signal model.

I. INTRODUCTION

As wireless communications have advanced from the first generation (1G) to 5G, the system capacity has been significantly increased by improving the transceiver designs, while the wireless channel has been considered to be uncontrollable. Recently, due to the advances in meta-materials, reconfigurable intelligent surfaces (RISs) have been proposed [1]–[4] for the purpose of intelligently controlling wireless channels to achieve improved communication performance. Specifically, an RIS is an array composed of a very large number of passive elements that reflects electromagnetic signals in a desired

manner so as to reconfigure the propagation properties of wireless environment [5]. Thanks to their high array gain, low cost, low power, and negligible noise [5]–[7], RISs promise to improve channel capacity [8], extend coverage [9], and save power [10] in future 6G networks. Additionally, RISs are also projected to have other applications such as in WiFi [11], precision measurement [12], and navigation [13].

As an important advantage of RIS, the negligible noise introduced by passive RISs enables a “square-law” array gain. Specifically, the array gain of an N -element RIS is proportional to N^2 , which is N times larger than that achievable by a standard N -antenna massive multiple-input multiple-output (MIMO) base station (BS) [14]. Benefiting from this advantage, RISs are expected to introduce significant capacity gains in wireless systems [8]. However, in practice, these capacity gains are typically only observed in communication scenarios where the direct link between transmitter and receiver is completely blocked or very weak [8]–[10], [15]–[17]. By contrast, in many scenarios where the direct link is not weak, conventional RISs can achieve only negligible capacity gains [18]. The reason behind this phenomenon is the “multiplicative fading” effect introduced by RISs, i.e., the equivalent path loss of the transmitter-RIS-receiver link is the product (instead of the sum) of the path losses of the transmitter-RIS and RIS-receiver links, which is usually thousands of times larger than that of the direct link [18]. As a result, the “multiplicative fading” effect makes it almost impossible for passive RISs to achieve noticeable capacity gains in many wireless environments. Many existing works on RISs have bypassed this effect by only considering scenarios with severely obstructed direct links [8]–[10], [15]–[17]. Therefore, to advance the practicability of RISs in future 6G wireless networks, a critical issue for RISs to be addressed is: *How to break the fundamental performance bottleneck caused by the “multiplicative fading” effect?*

To overcome the fundamental physical limitation imposed by the “multiplicative fading” effect, the new concept of active RIS is proposed in this paper. Specifically, our contributions are summarized as follows:

- To break the fundamental performance bottleneck of conventional passive RISs, we propose the concept of *active* RISs to overcome the “multiplicative fading” effect. Different from the existing *passive* RISs that passively reflect signals without amplification, the key feature of active RISs is their ability to actively reflect signals with amplification at the expense of additional power consumption, which can be realized by integrating reflection-type amplifiers into their reflecting elements.
- We develop a new signal model for the proposed active

Z. Zhang, L. Dai, X. Chen, C. Liu, and F. Yang are with the Department of Electronic Engineering as well as the Beijing National Research Center for Information Science and Technology (BNRist), Tsinghua University, Beijing 100084, China (e-mails: zhangzj20@mails.tsinghua.edu.cn, daill@tsinghua.edu.cn, cxb17@mails.tsinghua.edu.cn, liuch17@mails.tsinghua.edu.cn, fan_yang@tsinghua.edu.cn).

R. Schober is with the Institute for Digital Communications at Friedrich-Alexander University Erlangen-Nürnberg (FAU) (e-mail: robert.schober@fau.de).

H. V. Poor is with the Department of Electrical and Computer Engineering, Princeton University, USA (e-mail: poor@princeton.edu).

This work was supported in part by the National Key Research and Development Program of China (Grant No. 2020YFB1807201), in part by the National Natural Science Foundation of China (Grant No. 62031019), and in part by the U.S. National Science Foundation under Grants CCF-0939370 and CCF-1908308.

RISs, which characterizes the amplification of the incident signal and accounts for the non-negligible thermal noise introduced by the active elements. For verification, an active RIS element was designed and fabricated to validate the developed signal model via experimental measurements. Based on the developed signal model, we further analyze the asymptotic performance of active RISs and compare it to that of the existing passive RISs, which reveals the notable capacity gain enabled by the use of active RISs.

- To evaluate the performance of active RISs in typical communication systems, we formulate a sum-rate maximization problem for an active RIS aided MIMO system. Then, a joint transmit beamforming and reflect precoding algorithm is proposed to solve this problem. Simulation results show that, in a typical wireless system, the existing passive RISs achieve only a negligible sum-rate gain of 3%, while the proposed active RISs are able to achieve a substantial sum-rate gain of 67%, thus overcoming the “multiplicative fading” effect.

The rest of this paper is organized as follows. In Section II, the concept of active RISs is introduced, and a signal model for active RIS is developed. In Section III, the asymptotic performance of active RISs is analyzed and compared to that of the existing passive RISs. In Section IV, a sum-rate maximization problem is formulated, and a joint beamforming and precoding design for capacity maximization is proposed to solve the formulated problem. In Section V, experimental measurements are presented to validate the developed signal model, and numerical simulation results are provided to evaluate the performance of active RISs in typical communication scenarios. Finally, conclusions are drawn and future works are discussed in Section VI.

Notations: \mathbb{C} , \mathbb{R} , and \mathbb{R}_+ denote the sets of complex, real, and positive real numbers, respectively; $[\cdot]^{-1}$, $[\cdot]^T$, and $[\cdot]^H$ denote the inverse, transpose, and conjugate-transpose operations, respectively; $\|\cdot\|$ denotes the Frobenius norm of the argument; $\text{diag}(\cdot)$ denotes the diagonalization operation; $\Re\{\cdot\}$ denotes the real part of the argument; \otimes denotes the Kronecker product; $\angle[\cdot]$ denotes the angle of the complex argument; $\ln(\cdot)$ denotes the natural logarithm of its argument; $\mathcal{CN}(\boldsymbol{\mu}, \boldsymbol{\Sigma})$ denotes the complex multivariate Gaussian distribution with mean $\boldsymbol{\mu}$ and variance $\boldsymbol{\Sigma}$; \mathbf{I}_L is an $L \times L$ identity matrix, and $\mathbf{0}_L$ is an $L \times 1$ zero vector.

II. CONCEPT OF ACTIVE RIS

In this section, we introduce the concept of active RISs. First, in Subsection II-A, we review the existing passive RISs, and point out their fundamental physical limitation imposed by the “multiplicative fading” effect. Then, in Subsection II-B, to overcome this limitation, we propose the concept of active RISs along with their hardware structure and signal model. Finally, in Subsection II-C, we present the transmission model for an active RIS aided MIMO system.

A. Existing Passive RISs

The RISs widely studied in most existing works are passive RISs [1]–[10]. Specifically, as shown in Fig. 1 (a), a passive

RIS comprises a large number of passive elements each being able to reflect the incident signal with a controllable phase shift. In general, each passive RIS element consists of a reflective patch terminated with an impedance-adjustable circuit for phase shifting [19]. Thanks to the passive mode of operation without active radio-frequency (RF) components, a passive RIS element practically consumes zero direct-current power [19], and the introduced thermal noise is usually negligible [5]–[10]. Thereby, the signal model of an N -element passive RIS widely used in the literature is given as follows [6]

$$\mathbf{y} = \Theta \mathbf{x}, \quad (1)$$

where $\mathbf{x} \in \mathbb{C}^N$ denotes the incident signal, $\Theta := \text{diag}(e^{j\theta_1}, \dots, e^{j\theta_N}) \in \mathbb{C}^{N \times N}$ denotes the phase shift matrix of the RIS, and $\mathbf{y} \in \mathbb{C}^N$ denotes the signal reflected by the RIS. Note that the impact of noise is neglected in (1). As a consequence, by properly adjusting Θ to manipulate the N signals reflected by the N RIS elements to coherently add with the same phase at the receiver, a high array gain proportional to N^2 can be achieved. This is expected to significantly increase the receiver signal-to-noise ratio (SNR) [5]–[7], which is one of the key reasons for why RISs have attracted so much research interest recently [8]–[13], [15]–[17].

Unfortunately, in practice, this expected high capacity gain often cannot be realized, especially in communication scenarios where the direct link between the transmitter and the receiver is not weak. The reason for this negative result is the “multiplicative fading” effect introduced by passive RISs. Specifically, the equivalent path loss of the transmitter-RIS-receiver reflected link is the product (instead of the sum) of the path losses of the transmitter-RIS and RIS-receiver links, and therefore, it is thousands of times larger than that of the unobstructed direct link. Thereby, for an RIS to realize a noticeable capacity gain, thousands of RIS elements are required to compensate for this extremely large path loss.

Remark 1: To illustrate the above fact, let us consider a single-input single-output (SISO) system aided by a passive RIS with elements spaced by half a wavelength [20]. Let $d = 200$ m, $d_t = 150$ m, and $d_r = 200$ m denote the distances between transmitter and receiver, transmitter and RIS, RIS and receiver, respectively. For carrier frequencies of 5/10/20 GHz, according to the RIS “multiplicative fading” model in [18], $N = 10000/20000/40000$ RIS elements are required to make the reflected link as strong as the direct link. The high signaling overhead introduced by the N pilots required for channel estimation [21] and the high complexity of $\mathcal{O}(N^2)$ for real-time beamforming [22] make the application of such a large number of passive RIS elements in practical wireless networks very challenging [18]. Consequently, many existing works have bypassed the “multiplicative fading” effect by only considering the scenario where the direct link is completely blocked or very weak [5]–[10], [15]–[17].

B. Proposed Active RISs

To overcome the fundamental performance bottleneck caused by the “multiplicative fading” effect of RISs, we propose the concept of active RISs as a promising solution.

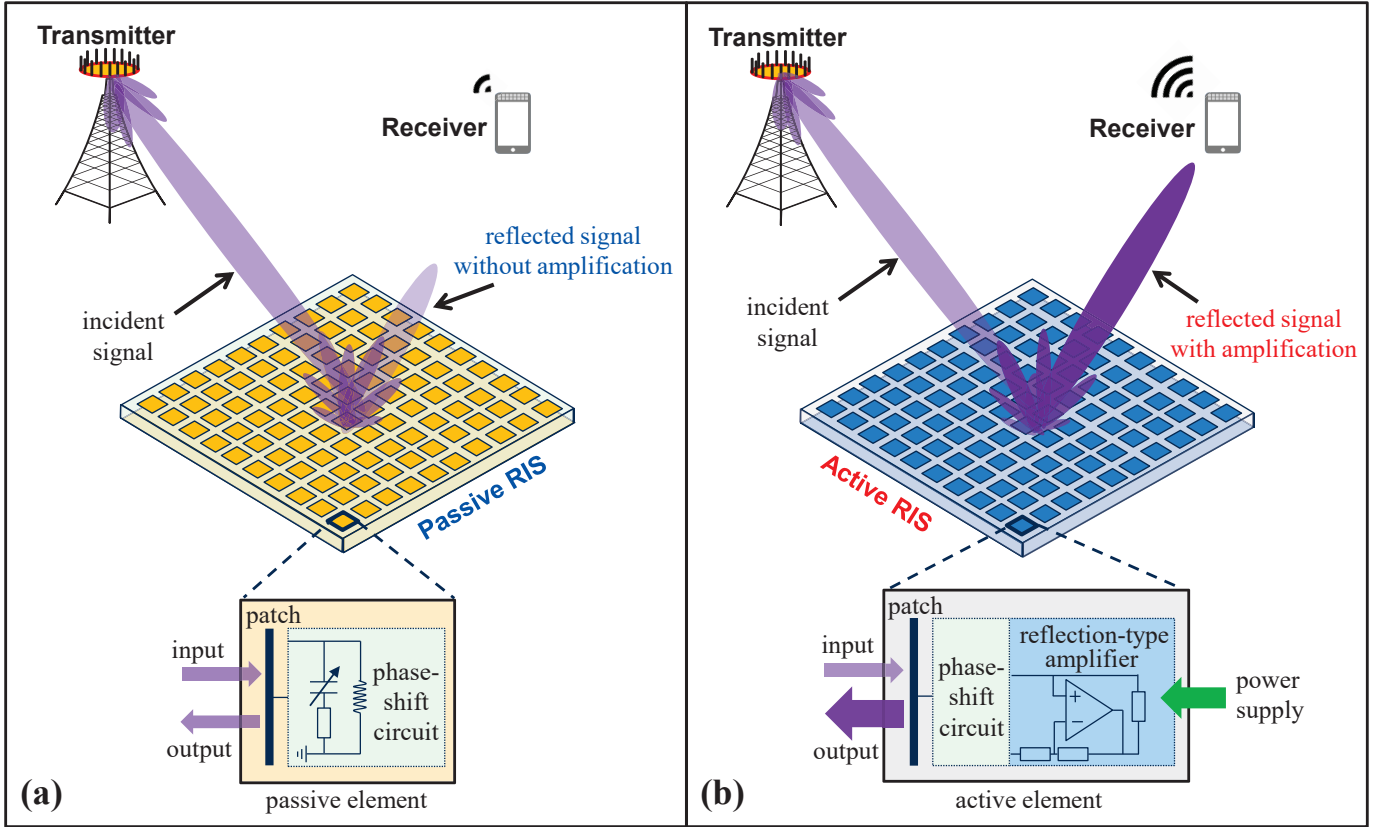


Fig. 1. Comparison between (a) the existing passive RIS and (b) the proposed active RIS.

As shown in Fig. 1 (b), similar to the existing passive RISs, active RISs can also reflect the incident signals with reconfigurable phase shifts. Different from passive RISs that just reflect the incident signals without amplification, active RISs can further amplify the reflected signals. To achieve this goal, the key component of an active RIS element is the additionally integrated active reflection-type amplifier, which can be realized by different existing active components, such as current-inverting converters [23], asymmetric current mirrors [24], or some integrated circuits [25].¹

With reflection-type amplifiers supported by a power supply, the reflected and amplified signal of an N -element active RIS can be modeled as follows:

$$\mathbf{y} = \underbrace{\mathbf{P}\Theta\mathbf{x}}_{\text{Desired signal}} + \underbrace{\mathbf{P}\Theta\mathbf{v}}_{\text{Dynamic noise}} + \underbrace{\mathbf{n}_s}_{\text{Static noise}}, \quad (2)$$

where $\mathbf{P} := \text{diag}(p_1, \dots, p_N) \in \mathbb{R}_+^{N \times N}$ denotes the amplification factor matrix of the active RIS, wherein each element p_n can be larger than one thanks to the integrated reflection-type amplifier. Due to the use of active components, active RISs consume additional power for amplifying the reflected signals, and the thermal noise introduced by active RIS elements cannot be neglected as is done for passive RISs. Particularly, as shown in (2), the introduced noise can be classified into dynamic noise and static noise [24]. Specifically, \mathbf{v} is related to the input noise and the inherent device noise of the active RIS

¹In this paper, we focus on studying reflective active RISs, while the investigation of transmissive active RISs is left for future work [26]–[28].

elements [24], while the static noise \mathbf{n}_s is unrelated to \mathbf{P} and is usually negligible compared to the dynamic noise $\mathbf{P}\Theta\mathbf{v}$, as will be verified by experimental results in Section V-A. Thus, here we neglect \mathbf{n}_s and model \mathbf{v} as $\mathbf{v} \sim \mathcal{CN}(\mathbf{0}_N, \sigma_v^2 \mathbf{I}_N)$.

Remark 2: Note that the proposed active RISs are fundamentally different from the relay-type RISs equipped with RF components [29]–[31] and relays [32]. Specifically, in [29]–[31], a subset of the passive RIS elements are connected to active RF chains, which are used for sending pilot signals and processing baseband signals. Thus, these relay-type RIS elements have signal processing capabilities [29]–[31]. On the contrary, the proposed active RISs do not have such capabilities but only reflect and amplify the incident signals to strengthen the reflected link. Besides, although the proposed active RISs can amplify the incident signals, similar to full-duplex amplify-and-forward (FD-AF) relays, their respective hardware architectures and transmission models are quite different. Specifically, an FD-AF relay is equipped with RF chains to receive the incident signal and then transmit it after amplification [32]. Due to the long delay inherent to this process, two time slots are needed to complete the transmission of one symbol, and the received signal at the receiver in a time slot actually depends on two different symbols, which were transmitted by the transmitter and the FD-AF relay, respectively [32]. As a consequence, in order to efficiently decode the symbols, the receiver in an FD-AF relay aided system has to combine the signals received in two successive time slots to maximize the SNR. Thus, the transmission

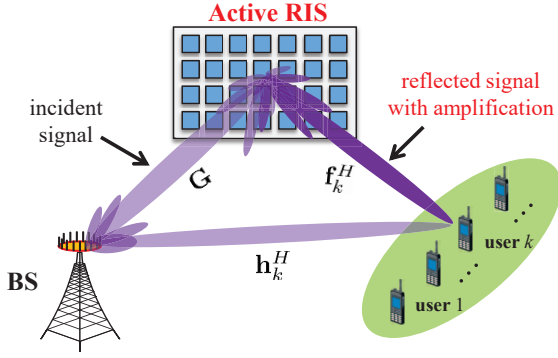


Fig. 2. An illustration of the downlink transmission in an active RIS aided MIMO system.

model for FD-AF relaying [32, Eq. (22), Eq. (25)] differs substantially from that for active RIS (4), which also leads to different achievable rates [32, Table I].

C. Active RIS Aided MIMO System

To characterize the performance gains enabled by active RISs in typical communication scenarios, we consider an active RIS aided downlink MIMO system as shown in Fig. 2, where an M -antenna BS serves K single-antenna users simultaneously with the aid of an N -element active RIS.

Let $\mathbf{s} := [s_1, \dots, s_K]^T \in \mathbb{C}^K$ denote the transmitted symbol vector for the K users with $\mathbb{E}\{\mathbf{s}\mathbf{s}^H\} = \mathbf{I}_K$. Assuming that multi-user linear precoding is employed at the BS for downlink transmission, the signal reflected by the active RIS, \mathbf{y} , can be modeled as follows:

$$\mathbf{y} = \mathbf{P}\mathbf{O}\mathbf{G} \sum_{j=1}^K \mathbf{w}_j s_j + \mathbf{P}\mathbf{O}\mathbf{v}, \quad (3)$$

where $\mathbf{G} \in \mathbb{C}^{N \times M}$ denotes the channel matrix between the BS and the RIS and $\mathbf{w}_k \in \mathbb{C}^{M \times 1}$ denotes the BS beamforming vector for symbol s_k . Thus, according to (3), signal $r_k \in \mathbb{C}$ received at user k can be modeled as follows:

$$\begin{aligned} r_k &= \mathbf{h}_k^H \sum_{j=1}^K \mathbf{w}_j s_j + \mathbf{f}_k^H \mathbf{y} + z_k \\ &= \underbrace{\left(\mathbf{h}_k^H \right)}_{\text{Direct link}} + \underbrace{\left(\mathbf{f}_k^H \mathbf{P}\mathbf{O}\mathbf{G} \right)}_{\text{Reflected link}} \sum_{j=1}^K \mathbf{w}_j s_j + \underbrace{\left(\mathbf{f}_k^H \mathbf{P}\mathbf{O}\mathbf{v} \right)}_{\text{Noise introduced by active RIS}} \\ &\quad + \underbrace{z_k}_{\text{Noise introduced at user } k}, \end{aligned} \quad (4)$$

where $\mathbf{h}_k^H \in \mathbb{C}^{1 \times M}$ and $\mathbf{f}_k^H \in \mathbb{C}^{1 \times N}$ denote the channel vector between the BS and user k and that between the RIS and user k , respectively; and z_k denotes the additive white Gaussian noise (AWGN) at user k with zero mean and variance σ^2 .

To analytically illustrate how the proposed active RISs can overcome the ‘‘multiplicative fading’’ effect, based on the signal model in (2), the performance gain enabled by the use of active RISs will be studied in the next section.

III. PERFORMANCE ANALYSIS

In this section, we analyze the performance of the proposed active RISs to reveal their notable capacity gains. To this end, in order to make the problem analytically tractable and get insightful results, in this section, we consider a single-input single-output (SISO) system with $M = 1$ BS antenna and $K = 1$ user, while the general MIMO case is studied in Section IV. In Subsection III-A, the asymptotic SNRs of a passive RIS aided system and an active RIS aided system are provided. Then, in Subsection III-B, to show the superiority of active RISs, the derived asymptotic SNRs for the two systems are compared.

A. Asymptotic SNR for Passive RISs and Active RISs

To illustrate the capacity gain provided by passive/active RIS aided reflected links, for the moment, we ignore the direct link by setting \mathbf{h}_k to zero, as was done in, e.g., [33]. Furthermore, for simplicity, we assume that each active RIS element has the same amplification factor (i.e., $p_n := p$ for all $n \in \{1, \dots, N\}$). For a fair comparison with the asymptotic performance of passive RISs, similar to [33], we assume Rayleigh-fading channels. This assumption has also been widely used for the performance analysis of massive MIMO systems, e.g., [14] and [34].

For the above RIS aided SISO system without direct link, we first redefine the BS-RIS channel matrix and the RIS-user channel vector as $\mathbf{G} := \mathbf{g} \in \mathbb{C}^{N \times 1}$ and $\mathbf{f}_k := \mathbf{f} \in \mathbb{C}^{N \times 1}$, respectively, to simplify the notations. Then, we recall the following lemma from [33] for the asymptotic SNR achieved by the existing passive RISs.

Lemma 1 (Asymptotic SNR for passive RISs): Assuming $\mathbf{f} \sim \mathcal{CN}(\mathbf{0}_N, \varrho_f^2 \mathbf{I}_N)$, $\mathbf{g} \sim \mathcal{CN}(\mathbf{0}_N, \varrho_g^2 \mathbf{I}_N)$ and letting $N \rightarrow \infty$, the asymptotic SNR γ_{passive} of a passive RIS aided SISO system is given by

$$\gamma_{\text{passive}} \rightarrow N^2 \frac{P_{\text{BS}}^{\max} \pi^2 \varrho_f^2 \varrho_g^2}{16\sigma^2}, \quad (5)$$

where P_{BS}^{\max} denotes the maximum transmit power at the BS.

Proof: The proof can be found in [33]. ■

For comparison, under the same transmission conditions, we provide the asymptotic SNR of an active RIS aided SISO system in the following lemma.

Lemma 2 (Asymptotic SNR for active RISs): Assuming $\mathbf{f} \sim \mathcal{CN}(\mathbf{0}_N, \varrho_f^2 \mathbf{I}_N)$, $\mathbf{g} \sim \mathcal{CN}(\mathbf{0}_N, \varrho_g^2 \mathbf{I}_N)$ and letting $N \rightarrow \infty$, the asymptotic SNR γ_{active} of an active RIS aided SISO system is given by

$$\gamma_{\text{active}} \rightarrow N \frac{P_{\text{BS}}^{\max} P_{\text{A}}^{\max} \pi^2 \varrho_f^2 \varrho_g^2}{16 \left(P_{\text{A}}^{\max} \sigma_v^2 \varrho_f^2 + P_{\text{BS}}^{\max} \sigma^2 \varrho_g^2 + \sigma^2 \sigma_v^2 \right)}, \quad (6)$$

where P_{A}^{\max} denotes the maximum reflect power of the active RIS.

Proof: Please see Appendix A. ■

Remark 3: From (6) we observe that the asymptotic SNR of an active RIS aided SISO system depends on both the BS transmit power P_{BS}^{\max} and the reflect power of the active RIS P_{A}^{\max} . Particularly, when $P_{\text{BS}}^{\max} \rightarrow \infty$, it is easy to

prove that the asymptotic SNR will be upper-bounded by $\gamma_{\text{active}} \rightarrow N \frac{P_{\text{A}}^{\max} \pi^2 \varrho_f^2}{16\sigma_v^2}$, which only depends on the RIS-user channel gain ϱ_f^2 and the noise power at the user σ^2 . This indicates that, when the BS transmit power is high enough, the BS-RIS channel \mathbf{g} and the noise power at the active RIS σ_v^2 have negligible impact on the user's SNR. Similarly, if $P_{\text{A}}^{\max} \rightarrow \infty$, the asymptotic SNR will be upper-bounded by $\gamma_{\text{active}} \rightarrow N \frac{P_{\text{BS}}^{\max} \pi^2 \varrho_g^2}{16\sigma_v^2}$, which is independent of the RIS-user channel \mathbf{f} and the noise power at the user σ^2 . These results reveal that to increase the sum-rate of active RIS aided systems, the negative impact of small \mathbf{g} and large σ_v^2 on system performance can be alleviated by increasing the BS transmit power P_{BS}^{\max} , and that of small \mathbf{f} and large σ^2 can be reduced by increasing the reflect power of the active RIS P_{A}^{\max} , which may provide guidance for the design of practical active RIS-aided systems.

Next, we compare the asymptotic SNRs for passive RISs in *Lemma 1* and active RISs in *Lemma 2* to reveal the superiority of active RISs in wireless communications.

B. Comparisons between Passive RISs and Active RISs

We can observe from *Lemma 1* and *Lemma 2* that, compared to the asymptotic SNR for passive RISs γ_{passive} in (5) which is proportional to N^2 , the asymptotic SNR for active RISs γ_{active} in (6) is proportional to N due to the noises additionally introduced by the use of active components. At first glance, it seems that the SNR proportional to N^2 achieved by passive RISs γ_{passive} always exceeds the SNR proportional to N achieved by active RISs γ_{active} . However, this is actually not the case. The reason behind this counterintuitive behavior is that, due to the large path loss caused by the ‘‘multiplicative fading’’ effect and thanks to the use of the reflection-type amplifiers in active RISs, only when N is unaffordably large can passive RISs outperform active RISs.

To illustrate this claim, let us consider two different SISO systems, which are aided by an active RIS and a passive RIS, respectively. Then, the following lemma specifies the condition that has to be met for passive RISs to outperform active RISs.

Lemma 3 (Case when passive RISs outperform active RISs): Assuming the number of RIS elements N is large, the required number of elements N for a passive RIS to outperform an active RIS has to satisfy

$$N \geq \frac{P_{\text{BS-A}}^{\max}}{P_{\text{BS-P}}^{\max}} \frac{P_{\text{A}}^{\max} \sigma^2}{\left(P_{\text{A}}^{\max} \sigma_v^2 \varrho_f^2 + P_{\text{BS-A}}^{\max} \sigma^2 \varrho_g^2 + \sigma^2 \sigma_v^2 \right)}, \quad (7)$$

where $P_{\text{BS-A}}^{\max}$ denotes the maximum BS transmit power for the active RIS aided system and $P_{\text{BS-P}}^{\max}$ denotes that for the passive RIS aided system.

Proof: Please see Appendix B. ■

Next, we consider a specific setup to compare the user's achievable SNRs in the above two systems. For a fair comparison, we constrain the total power consumption P^{\max} of the two systems to 2 W by setting $P_{\text{BS-P}}^{\max} = 2$ W for the passive RIS aided system and $P_{\text{BS-A}}^{\max} = P_{\text{A}}^{\max} = 1$ W for the active RIS aided system, respectively. Therefore, when $\sigma^2 = \sigma_v^2 = -70$ dBm and $\varrho_f^2 = \varrho_g^2 = -70$ dB, the required

number of elements N for the passive RIS to outperform the active RIS is 2.5×10^6 according to (7), which is impractical to realize with current technology. Conversely, for a more practical number of elements of $N = 256$, according to (6) and (5), the SNR achieved by the passive RIS is $\gamma_{\text{passive}} \approx 9.0$ dB, while the SNR achieved by the active RIS is $\gamma_{\text{active}} \approx 49.0$ dB, which is about 10,000 times higher than γ_{passive} .

To further illustrate our findings, we show the asymptotic SNR versus the number of RIS elements N for both passive RISs and active RISs in Fig. 3, where N ranges from 10 to 1000 in Fig. 3 (a) and from 10^4 to 3×10^6 in Fig. 3 (b). From this figure we can observe that, when N ranges from 10 to 1000, the user's achievable SNR is about 40 dB higher in an active RIS aided system compared to a passive RIS aided system. Only when $N = 2.5 \times 10^6$ becomes the performance gain achieved by the passive RIS comparable to that achieved by the active RIS, which agrees well with our above analysis.

Remark 4: From the above comparisons we find that, although additional thermal noise is introduced by the active components, active RISs can still achieve a higher SNR than passive RISs. This is due to the fact that the desired signals reflected by different active RIS elements are coherently added with the same phase at the user, while the introduced noises are not. This is the reason for the capacity improvement achieved by active RISs. To further support this insight, more simulation results will be presented in Section V.

IV. JOINT TRANSMIT BEAMFORMING AND REFLECT PRECODING DESIGN

To investigate the capacity gain enabled by the use of active RISs in typical wireless communication scenarios, in this section, we consider more general MIMO systems. Specifically, in Subsection IV-A, we first formulate the problem of sum-rate maximization for an active RIS aided MIMO system. Then, in Subsection IV-B, the proposed joint transmit beamforming and reflect precoding algorithm to solve the problem is introduced. Finally, in Subsection IV-C, the convergence and computational complexity of the proposed algorithm are discussed.

A. Capacity Maximization Problem Formulation

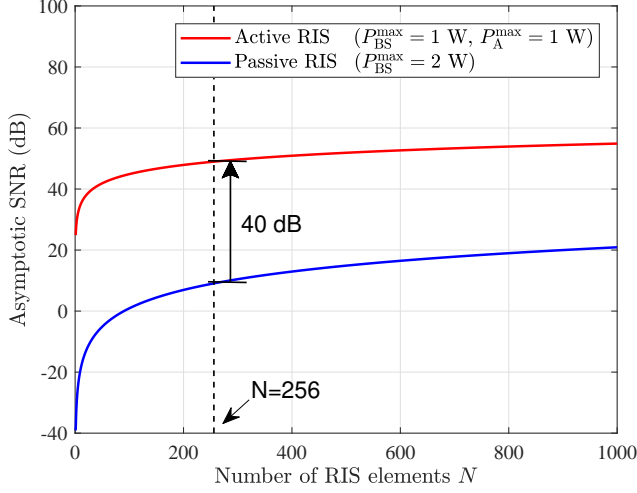
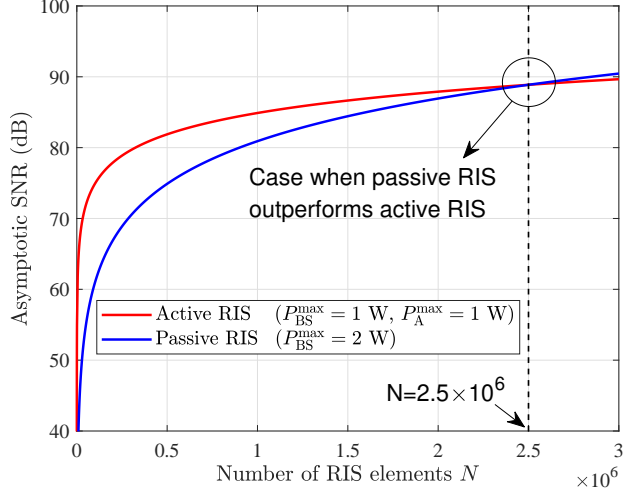
According to the multi-user MIMO transmission model in (4), the signal-to-interference-plus-noise ratio (SINR) at user k can be obtained as

$$\gamma_k = \frac{|\bar{\mathbf{h}}_k^H \mathbf{w}_k|^2}{\sum_{j=1, j \neq k}^K |\bar{\mathbf{h}}_k^H \mathbf{w}_j|^2 + \|\mathbf{f}_k^H \mathbf{P} \Theta\|^2 \sigma_v^2 + \sigma^2}, \quad (8)$$

wherein $\bar{\mathbf{h}}_k^H = \mathbf{h}_k^H + \mathbf{f}_k^H \mathbf{P} \Theta \mathbf{G} \in \mathbb{C}^{1 \times M}$ is the equivalent channel from the BS to user k , which includes both the direct link and the reflected link. Similarly, the BS transmit power, P_{BS} , and the reflect power of the active RIS, P_{A} , can be respectively expressed as

$$P_{\text{BS}} = \sum_{k=1}^K \|\mathbf{w}_k\|^2, \quad (9a)$$

$$P_{\text{A}} = \sum_{k=1}^K \|\mathbf{P} \Theta \mathbf{G} \mathbf{w}_k\|^2 + \|\mathbf{P} \Theta\|^2 \sigma_v^2. \quad (9b)$$

(a) N ranges from 10 to 1000.(b) N ranges from 10^4 to 3×10^6 .Fig. 3. Asymptotic SNR as a function of the number of RIS elements N for different ranges of N .

Therefore, the original problem of sum-rate maximization, subject to the power constraints at the BS and the active RIS, can be formulated as follows:

$$\mathcal{P}_o : \max_{\mathbf{w}, \mathbf{P}, \Theta} R_{\text{sum}}(\mathbf{w}, \mathbf{P}, \Theta) = \sum_{k=1}^K \log_2(1 + \gamma_k), \quad (10a)$$

$$\text{s.t. } C_1 : \sum_{k=1}^K \|\mathbf{w}_k\|^2 \leq P_{\text{BS}}^{\max}, \quad (10b)$$

$$C_2 : \sum_{k=1}^K \|\mathbf{P}\Theta\mathbf{G}\mathbf{w}_k\|^2 + \|\mathbf{P}\Theta\|^2 \sigma_v^2 \leq P_A^{\max}, \quad (10c)$$

where $\mathbf{w} := [\mathbf{w}_1^T, \dots, \mathbf{w}_K^T]^T$ is the overall transmit beamforming vector for the K users; C_1 and C_2 are the power constraints at the BS and active RIS, respectively. Due to the non-convexity and highly coupled variables in problem \mathcal{P}_o in (10), the joint design of \mathbf{w} , \mathbf{P} , and Θ is challenging. To efficiently solve this problem, in the next subsection, we develop a joint beamforming and precoding algorithm based on alternating optimization and fractional programming (FP).

B. Proposed Joint Beamforming and Precoding Algorithm

To solve the problem efficiently, we reformulate the problem first. Note that \mathbf{P} and Θ always appear in product form in problem \mathcal{P}_o in (10). Therefore, \mathbf{P} and Θ can be merged as $\Psi = \mathbf{P}\Theta = \text{diag}(p_1 e^{j\theta_1}, \dots, p_N e^{j\theta_N}) \in \mathbb{C}^{N \times N}$. Hence, optimizing \mathbf{P} and Θ is equivalent to optimizing Ψ . We refer to Ψ as the RIS precoding matrix. Next, to deal with the non-convex sum-of-logarithms and fractions in (10), we exploit FP methods proposed in [35] to decouple the variables in problem \mathcal{P}_o in (10). This leads to the following lemma.

Lemma 4 (Equivalent problem for sum-rate maximization): By introducing auxiliary variables $\rho := [\rho_1, \dots, \rho_K] \in$

\mathbb{R}_+^K and $\varpi := [\varpi_1, \dots, \varpi_K] \in \mathbb{C}^K$, the original problem \mathcal{P}_o in (10) can be equivalently reformulated as follows

$$\begin{aligned} \mathcal{P}_1 : \max_{\mathbf{w}, \Psi, \rho, \varpi} R'_{\text{sum}}(\mathbf{w}, \Psi, \rho, \varpi) &= \sum_{k=1}^K \ln(1 + \rho_k) - \\ &\quad \sum_{k=1}^K \rho_k + \sum_{k=1}^K g(\mathbf{w}, \Psi, \rho_k, \varpi_k), \quad (11) \\ \text{s.t. } C_1 : \|\mathbf{w}\|^2 &\leq P_{\text{BS}}^{\max}, \\ C_2 : \sum_{k=1}^K \|\Psi\mathbf{G}\mathbf{w}_k\|^2 + \|\Psi\|^2 \sigma_v^2 &\leq P_A^{\max}, \end{aligned}$$

where function $g(\mathbf{w}, \Psi, \rho_k, \varpi_k)$ is defined as

$$\begin{aligned} g(\mathbf{w}, \Psi, \rho_k, \varpi_k) &= 2\sqrt{(1 + \rho_k)} \Re \{ \varpi_k^* \bar{\mathbf{h}}_k^H \mathbf{w}_k \} - \\ &\quad |\varpi_k|^2 \left(\sum_{j=1}^K |\bar{\mathbf{h}}_k^H \mathbf{w}_j|^2 + \|\mathbf{f}_k^H \Psi\|^2 \sigma_v^2 + \sigma^2 \right). \quad (12) \end{aligned}$$

Proof: Please see Appendix C. ■

Strong convergence of the FP methods was proved in [35]. Thus, a locally optimal solution to (11) can be obtained by alternately optimizing the BS beamforming vector \mathbf{w} , RIS precoding matrix Ψ , auxiliary variables ρ and ϖ in (11), until R_{sum} converges. For clarity, we summarize the proposed joint beamforming and precoding algorithm in **Algorithm 1**, and the specific optimal solutions for variables \mathbf{w} , Ψ , ρ , and ϖ are given in the following four steps, respectively.

1) *Fix $(\mathbf{w}, \Psi, \varpi)$ and then optimize ρ :* After fixing BS beamforming vector \mathbf{w} , RIS precoding matrix Ψ , and auxiliary variable ϖ , the optimal ρ can be obtained by solving $\frac{\partial R'_{\text{sum}}}{\partial \rho_k} = 0$ as

$$\rho_k^{\text{opt}} = \frac{\xi_k^2 + \xi_k \sqrt{\xi_k^2 + 4}}{2}, \quad \forall k \in \{1, \dots, K\}, \quad (13)$$

where $\xi_k = \Re \{ \varpi_k^* \bar{\mathbf{h}}_k^H \mathbf{w}_k \}$.

Algorithm 1 Proposed joint transmit beamforming and reflect precoding algorithm

Input: Channels \mathbf{G} , \mathbf{h}_k , and \mathbf{f}_k , $\forall k \in \{1, \dots, K\}$.
Output: Optimized BS beamforming vector \mathbf{w} , amplification factor matrix of active RIS \mathbf{P} , phase shift matrix of active RIS $\mathbf{\Theta}$, and sum-rate R_{sum} .

- 1: Randomly initialize \mathbf{w} , \mathbf{P} and $\mathbf{\Theta}$;
- 2: **while** no convergence of R_{sum} **do**
- 3: Update ρ by (13);
- 4: Update ϖ by (14);
- 5: Update \mathbf{w} by solving (16);
- 6: Update $\mathbf{\Psi}$ by solving (18);
- 7: Update R_{sum} by (10a);
- 8: **end while**
- 9: Obtain \mathbf{P} and $\mathbf{\Theta}$ from $\mathbf{\Psi}$;
- 10: **return** Optimized \mathbf{w} , \mathbf{P} , $\mathbf{\Theta}$, and R_{sum} .

2) Fix $(\mathbf{w}, \mathbf{\Psi}, \rho)$ and then optimize ϖ : After fixing the BS beamforming vector \mathbf{w} , RIS precoding matrix $\mathbf{\Psi}$, and auxiliary variable ρ , the optimal ϖ can be derived by solving $\frac{\partial R'_{\text{sum}}}{\partial \varpi_k} = 0$ as

$$\varpi_k^{\text{opt}} = \frac{\sqrt{(1 + \rho_k) \bar{\mathbf{h}}_k^H \mathbf{w}_k}}{\sum_{j=1}^K |\bar{\mathbf{h}}_k^H \mathbf{w}_j|^2 + \|\mathbf{f}_k^H \mathbf{\Psi}\|^2 \sigma_v^2 + \sigma^2}, \quad (14)$$

$\forall k \in \{1, \dots, K\}$.

3) Fix $(\mathbf{\Psi}, \rho, \varpi)$ and then optimize \mathbf{w} : To simplify the notations, we first introduce the following definitions:

$$\mathbf{b}_k^H = 2\sqrt{(1 + \rho_k) \varepsilon_k^* \bar{\mathbf{h}}_k^H}, \quad \mathbf{b} = [\mathbf{b}_1^T, \mathbf{b}_2^T, \dots, \mathbf{b}_N^T]^T, \quad (15a)$$

$$\mathbf{A} = \mathbf{I}_K \otimes \sum_{k=1}^K |\varepsilon_k|^2 \bar{\mathbf{h}}_k \bar{\mathbf{h}}_k^H, \quad \mathbf{\Xi} = \mathbf{I}_K \otimes (\mathbf{G}^H \mathbf{\Psi}^H \mathbf{\Psi} \mathbf{G}), \quad (15b)$$

$$P_m^{\text{max}} = P_A^{\text{max}} - \|\mathbf{\Psi}\|^2 \sigma_v^2. \quad (15c)$$

Then, for fixed RIS precoding matrix $\mathbf{\Psi}$ and auxiliary variables ρ and ϖ , problem \mathcal{P}_1 in (11) can be reformulated as follows

$$\mathcal{P}_2: \quad \max_{\mathbf{w}} \quad \Re\{\mathbf{b}^H \mathbf{w}\} - \mathbf{w}^H \mathbf{A} \mathbf{w},$$

s.t. $C_1: \|\mathbf{w}\|^2 \leq P_{\text{BS}}^{\text{max}},$ (16)

$C_2: \mathbf{w}^H \mathbf{\Xi} \mathbf{w} \leq P_m^{\text{max}}.$

Note that \mathcal{P}_2 in (16) is a standard quadratic constraint quadratic programming (QCQP) problem. Thus, by adopting the Lagrange multiplier method [36], the optimal solution \mathbf{w}^{opt} to \mathcal{P}_2 in (16) can be obtained as follows

$$\mathbf{w}^{\text{opt}} = (\mathbf{A} + \lambda_1 \mathbf{I}_{MK} + \lambda_2 \mathbf{\Xi})^{-1} \mathbf{b}, \quad (17)$$

where λ_1 and λ_2 are the Lagrange multipliers, which should be chosen such that the complementary slackness conditions of power constraints C_1 and C_2 are satisfied. The optimal Lagrange multipliers λ_1^{opt} and λ_2^{opt} can be obtained via a two-dimensional grid search [36].

4) Fix $(\mathbf{w}, \rho, \varpi)$ and then optimize $\mathbf{\Psi}$: Define $\psi = [p_1 e^{j\theta_1}, \dots, p_N e^{j\theta_N}]^H$ as the vectorized RIS precoding matrix $\mathbf{\Psi}$, i.e., $\text{diag}(\psi) := \mathbf{\Psi}$. While fixing BS beamforming

vector \mathbf{w} and auxiliary variables ρ and ϖ , problem \mathcal{P}_1 in (11) can be reformulated as follows:

$$\mathcal{P}_3: \quad \max_{\psi} \quad \Re\{\psi^H \mathbf{v}\} - \psi^H \mathbf{\Omega} \psi,$$

(18)

s.t. $C_2: \psi^H \mathbf{\Pi} \psi \leq P_A^{\text{max}},$

wherein

$$\mathbf{v} = 2 \sum_{k=1}^K \sqrt{(1 + \rho_k) \text{diag}(\varpi_k^* \mathbf{f}_k^H)} \mathbf{G} \mathbf{w}_k - \sum_{k=1}^K |\varpi_k|^2 \text{diag}(\mathbf{f}_k^H) \mathbf{G} \sum_{j=1}^K \mathbf{w}_j \mathbf{w}_j^H \mathbf{h}_k, \quad (19a)$$

$$\mathbf{\Omega} = \sum_{k=1}^K |\varpi_k|^2 \text{diag}(\mathbf{f}_k^H) \text{diag}(\mathbf{f}_k) \sigma_v^2 + \sum_{k=1}^K |\varpi_k|^2 \sum_{j=1}^K \text{diag}(\mathbf{f}_k^H) \mathbf{G} \mathbf{w}_j \mathbf{w}_j^H \mathbf{G}^H \text{diag}(\mathbf{f}_k), \quad (19b)$$

$$\mathbf{\Pi} = \sum_{k=1}^K \text{diag}(\mathbf{G} \mathbf{w}_k) (\text{diag}(\mathbf{G} \mathbf{w}_k))^H + \sigma_v^2 \mathbf{I}_N. \quad (19c)$$

Note that problem \mathcal{P}_3 in (18) is also a standard QCQP problem. Thus, the optimal solution ψ^{opt} can be obtained by adopting the Lagrange multiplier method [36] and is given by

$$\psi^{\text{opt}} = (\mathbf{\Omega} + \mu \mathbf{\Pi})^{-1} \mathbf{v}, \quad (20)$$

where μ is the Lagrange multiplier, which should be chosen such that the complementary slackness condition of power constrain C_2 is satisfied. Similarly, the optimal Lagrange multiplier μ^{opt} can be obtained via a binary search [36].

C. Discussion of Convergence and Complexity

In this subsection, we analyze the convergence and the computational complexity of the proposed joint beamforming and precoding design algorithm, respectively.

1) *Convergence*: The proposed joint beamforming and precoding design converges to a local optimal point after several iterations, since the updates in each iteration step of the algorithm, i.e., the updates of auxiliary variable ρ in (13), auxiliary variable ϖ in (14), BS beamforming vector \mathbf{w} in (16), and RIS precoding matrix $\mathbf{\Psi}$ in (18), are all optimal solutions to the respective subproblems, which cause the objective $R'_{\text{sum}}(\mathbf{w}, \mathbf{\Psi}, \rho, \varpi)$ to monotonically increase. To prove this, here we introduce superscript t as the iteration index in **Algorithm 1**, e.g., \mathbf{w}^t refers to the transmit beamforming vector at the end of the t -th iteration. Then, **Algorithm 1** converges as

$$R'_{\text{sum}}(\mathbf{w}^{t+1}, \mathbf{\Psi}^{t+1}, \rho^{t+1}, \varpi^{t+1}) \stackrel{(a)}{\geq} R'_{\text{sum}}(\mathbf{w}^{t+1}, \mathbf{\Psi}^t, \rho^{t+1}, \varpi^{t+1}) \stackrel{(b)}{\geq} R'_{\text{sum}}(\mathbf{w}^t, \mathbf{\Psi}^t, \rho^{t+1}, \varpi^{t+1}) \stackrel{(c)}{\geq} R'_{\text{sum}}(\mathbf{w}^t, \mathbf{\Psi}^t, \rho^{t+1}, \varpi^t) \stackrel{(d)}{\geq} R'_{\text{sum}}(\mathbf{w}^t, \mathbf{\Psi}^t, \rho^t, \varpi^t), \quad (21)$$

holds, where (a) and (b) follow since the updates of $\mathbf{\Psi}$ and \mathbf{w} are the optimal solutions to subproblems \mathcal{P}_3 in (18) and \mathcal{P}_2 in (16), respectively; (c) and (d) follow because the updates of

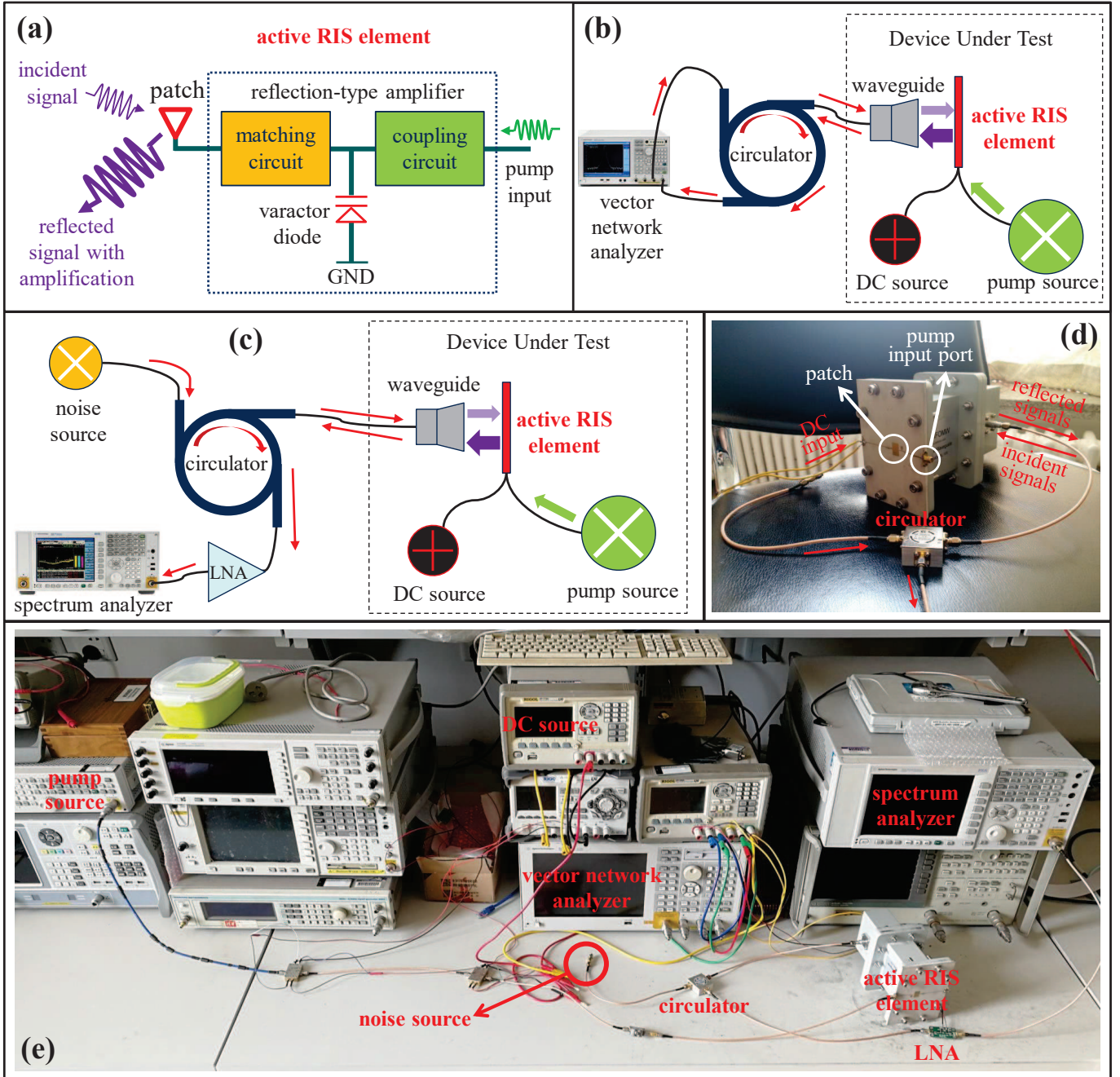


Fig. 4. The experimental devices and environment for validating the developed signal model (2) of the proposed active RIS.

ϖ and ρ maximize R'_{sum} when the other variables are fixed, respectively. Therefore, the objective R'_{sum} is monotonically non-decreasing in each iteration. Since the value of R'_{sum} is upper-bounded due to power constraints C_1 and C_2 , **Algorithm 1** will converge to a local optimum. Furthermore, the finally obtained \mathbf{w} and Ψ determine the local optimal solution to the original problem \mathcal{P}_o in (10).

2) *Computational complexity*: The overall computational complexity of the proposed algorithm is mainly determined by the updates of the four variables ρ , ϖ , \mathbf{w} , and Ψ via (13), (14), (16), and (18), respectively. Specifically, the computational complexity of updating ρ is $\mathcal{O}(KM)$, which is caused by the calculation of ξ_k as shown in (13). Sim-

ilarly, the complexity of updating ϖ is $\mathcal{O}(K^2M + KN)$, which is caused by the calculations of $\mathbf{h}_k^H \mathbf{w}_j$ and $\mathbf{f}_k^H \Psi$ as shown in (14). Different from the updates of ρ and ϖ , which have closed-form expressions, the updates of \mathbf{w} and Ψ require solving standard QCQP problems via the Lagrange multiplier method [36]. Thus, considering the complexity of solving standard QCQP problem [37], for a given accuracy tolerance ε , the computational complexity of updating \mathbf{w} is $\mathcal{O}(\log_2(1/\varepsilon) \sqrt{MK+2} (1+MK) M^3 K^3)$, which is due to the matrix inversion and the two-dimensional grid search for Lagrange multipliers λ_1 and λ_2 as shown in (17). Similarly, the computational complexity of updating Ψ is $\mathcal{O}(\log_2(1/\varepsilon) \sqrt{N+1} (1+2N) N^3)$, which is due to the ma-

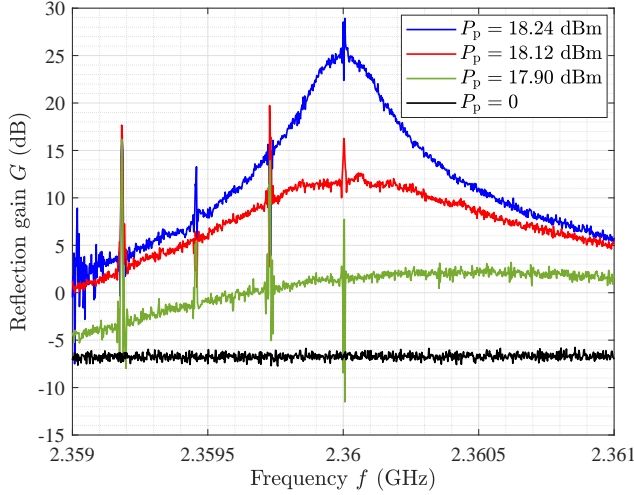


Fig. 5. Experimental measurement result for reflection gain G versus signal frequency f .

trix inversion and the binary search for Lagrange multiplier μ as shown in (20). Thus, the overall computational complexity of the proposed joint beamforming and precoding algorithm is given by $\mathcal{O}(\log_2(1/\varepsilon) I_o (M^{4.5} K^{4.5} + N^{4.5}))$, wherein I_o denotes the number of iterations required for convergence.

V. VALIDATION RESULTS

In this section, to validate the developed signal model (2), in Subsection V-A, we first present experimental results for a fabricated active RIS element. Then, in Subsection V-B, simulation results are provided to evaluate the performance of an active RIS aided MIMO system. Finally, in Subsection V-C, the impact of key system parameters on performance is discussed.

A. Validation Results for Signal Model

To validate the developed signal model (2), we designed and fabricated an active RIS element with an integrated reflection-type amplifier for experimental measurements² in [38]. Note that this design can be directly extended to the large-array case. Particularly, since the phase-shifting ability of RISs has been widely verified [19], we focus on studying the reflection gain and the noise introduced by an active RIS element. Thus, the validation of signal model (2) is equivalent to validating

$$P_y = \underbrace{GP_x}_{\text{Desired-signal power}} + \underbrace{G\sigma_v^2 + \sigma_s^2}_{\text{noise power}}, \quad (22)$$

where P_y is the power of the signals reflected by the active RIS element; P_x is the power of the incident signal; $G := p^2$ is the reflection gain of the active RIS element; $G\sigma_v^2$ and σ_s^2 are the powers of the dynamic noise and static noise introduced by the active RIS element, respectively.

²In October 2019, we started to design an active RIS element integrating a reflection-type amplifier [38]. The fabrication of this active RIS element was finished in August 2020. Subsequently, we set out to establish an experimental environment for signal measurements with this element, and all measurements were completed in February 2021.

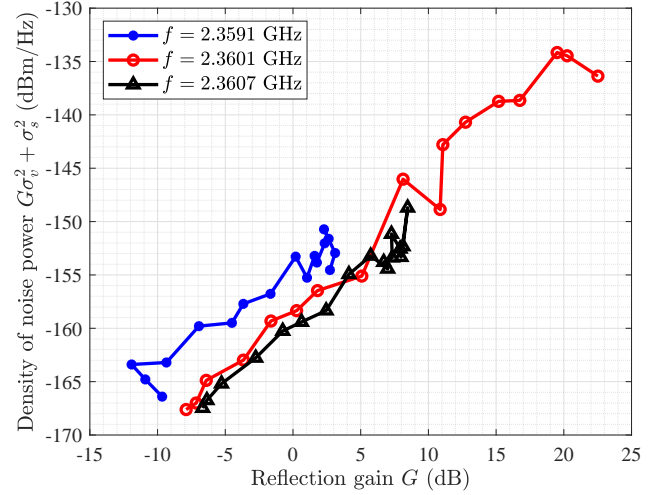


Fig. 6. Experimental measurement result for the density of noise power $G\sigma_v^2 + \sigma_s^2$ versus reflection gain G .

1) *Hardware platform:* To validate the model in (22), we first establish the hardware platform used for our experimental measurements, see Fig. 4. Specifically, we show the following aspects:

- Fig. 4 (a) illustrates the structure of the fabricated active RIS element operating at a frequency of 2.36 GHz [38]. A pump input at a frequency of 4.72 GHz is used to supply the power required by the active RIS element. The incident signal and the pump input are coupled in a varactor-diode-based reflection-type amplifier to generate the reflected signal with amplification.
- Fig. 4 (b) illustrates the system used for measuring the reflection gain G of the active RIS element. A direct-current (DC) source is used to provide a bias voltage of 7.25 V for driving the active RIS element, and a controllable pump source is used to reconfigure the reflection gain G . A circulator is used to separate the incident signal and the reflected signal, and the reflection gain is directly measured by a vector network analyzer.
- Fig. 4 (c) illustrates the system for measuring the noises introduced at the active RIS element, where a spectrum analyzer is used to measure the noise power. The noise source is a 50 Ω impedance, which aims to simulate a natural input noise of -174 dBm/Hz at each patch. The reflected signal is amplified by a low-noise amplifier (LNA) so that the spectrum analyzer can detect it.
- Fig. 4 (d) shows a photo of the fabricated active RIS element under test, which is connected by a waveguide for incident/reflected signal exchanges.
- Fig. 4 (e) shows a photo of the experimental environment with the required equipment for device driving and signal measurement.

2) *Reflection gain measurement:* Using the measurement system for the reflection gain depicted in Fig. 4 (b), we first investigate the reflection gain G of the active RIS element. Note that the reflection gain G can be reconfigured by the input power of the pump source P_p . By setting the input power of

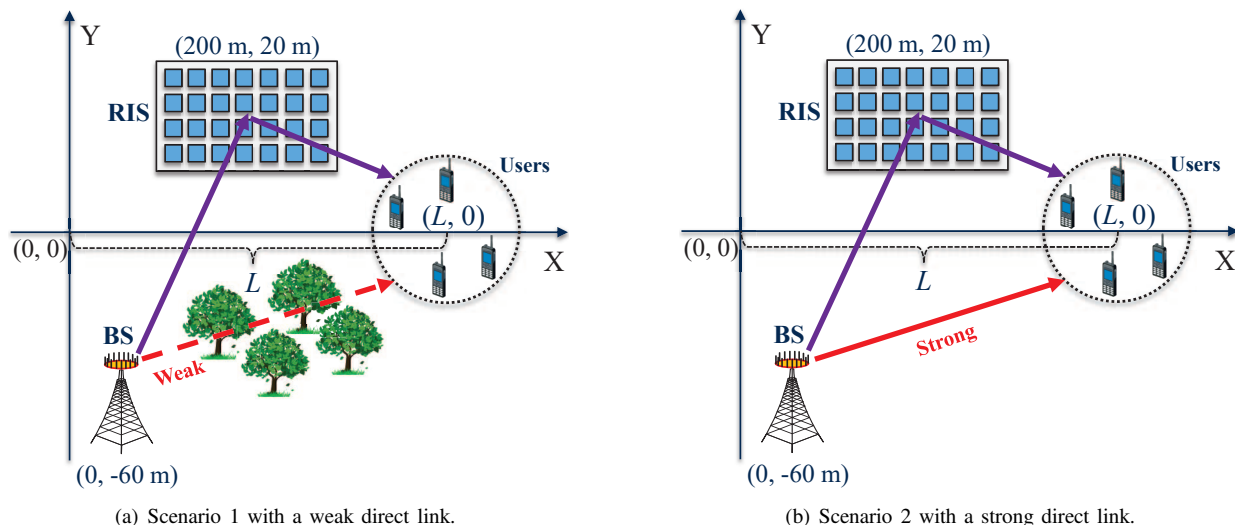


Fig. 7. Two simulation scenarios with different channel conditions, where a BS aided by an active RIS serves four users.

the vector network analyzer as $P_x = -50$ dBm, the reflection gain G as a function of the signal frequency can be directly measured via the vector network analyzer. Then, in Fig. 5, we show the measurement results for reflection gain G as a function of signal frequency f for different input powers of the pump source P_p . We observe that the active RIS element can achieve a reflection gain G of more than 25 dB, when $P_p = 18.24$ dBm, which confirms the significant reflection gains enabled by active RISs. On the other hand, when $P_p = 0$, we observe that G falls to -6 dB, which is lower than the expected 0 dB. This loss is mainly caused by the inherent power losses of the circulator and transmission lines used for measurement.

3) *Noise power measurement*: We further study the noise power introduced by the active RIS element, i.e., $G\sigma_v^2 + \sigma_s^2$ in (22), where $G\sigma_v^2$ and σ_s^2 are the powers of the dynamic noise and static noise introduced at the active RIS element, respectively. Using the noise measurement system in Fig. 4 (c), we show the measurement results for the spectral density of noise power $G\sigma_v^2 + \sigma_s^2$ as a function of G for different operating frequencies in Fig. 6. We can observe that the noise power increases nearly linearly with G , which verifies the noise model $G\sigma_v^2 + \sigma_s^2$ in (22). Particularly, for $f = 2.3601$ GHz, the spectral density of σ_s^2 is about -174 dBm/Hz, while that of σ_v^2 is about -160 dBm/Hz, which is about 15 dB higher. The reason for this is that the input noise is amplified by the noise factor [24], and additional noises are also introduced by the other active components the measurement equipment, such as the leakage noise from the DC source.

B. Simulation Results for Joint Beamforming and Precoding Design

To evaluate the performance of the proposed active RIS in typical wireless transmission scenarios, in this subsection, we present simulation results for passive RIS and active RIS aided MIMO systems, respectively.

1) *Simulation setup*: For the simulation setup, we consider an active RIS aided MIMO system operating at a frequency

of 5 GHz as shown in Fig. 7. Particularly, we consider two scenarios with different channel conditions. In Fig. 7 (a), the direct link is weak due to severe obstruction, while the direct link is strong in Fig. 7 (b). To be specific, two different path loss models from the 3GPP standard [39, B.1.2.1] are utilized to characterize the large-scale fading of the channels:

$$\begin{aligned} \text{PL}_s &= 37.3 + 22.0 \log d, \\ \text{PL}_w &= 41.2 + 28.7 \log d, \end{aligned} \quad (23)$$

where d is the distance between two devices. Path loss model PL_w is used to generate the weak BS-user link in scenario 1, while PL_s is used to generate the strong BS-user link in scenario 2. For both scenarios in Fig. 7, PL_s is used to generate the BS-RIS and the RIS-user channels. To account for small-scale fading, following [40], we adopt the Ricean fading channel model for all channels involved. In this way, an arbitrary channel matrix \mathbf{H} is generated by

$$\mathbf{H} = \sqrt{\text{PL}} \left(\sqrt{\frac{\kappa}{\kappa+1}} \mathbf{H}_{\text{LoS}} + \sqrt{\frac{1}{\kappa+1}} \mathbf{H}_{\text{NLoS}} \right), \quad (24)$$

where PL is the corresponding path loss of \mathbf{H} ; κ is the Ricean factor; and \mathbf{H}_{LoS} and \mathbf{H}_{NLoS} represent the deterministic LoS and Rayleigh fading components, respectively. In particular, here we assume $\kappa = 10$ [40].

As common settings, the BS and the active/passive RIS are located at $(0, -60$ m) and $(200$ m, 20 m), respectively. The four users are randomly located in a circle with a radius of 5 m from the center $(L, 0)$. Unless specified otherwise, the numbers of BS antennas and RIS elements are set as $M = 4$ and $N = 256$, respectively. The noise power is set as $\sigma^2 = \sigma_v^2 = -70$ dBm. For fair comparison, we constrain the total power consumption $P^{\max} := P_{\text{BS}}^{\max} + P_{\text{A}}^{\max}$ to 10 W by setting $P_{\text{BS}}^{\max} = P_{\text{A}}^{\max} = 5$ W for the active RIS aided system and $P_{\text{BS}}^{\max} = 10$ W for the benchmark system. For the active RIS, the proposed **Algorithm 1** is employed for joint beamforming and precoding design, while for the passive RIS, the joint beamforming and precoding algorithm from [22] is adopted.

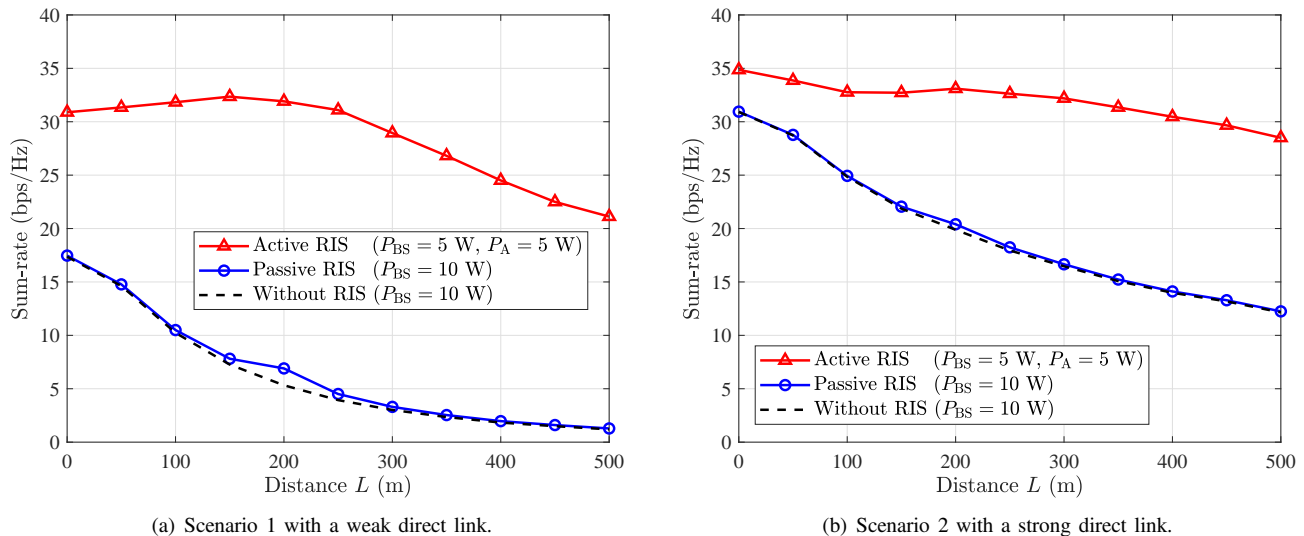


Fig. 8. Simulation results for the sum-rate as a function of distance L in an RIS-aided MIMO system.

2) *Simulation results*: In Fig. 8 (a) and (b), we plot the sum-rate versus distance L for the two considered scenarios, where the direct link is weak and strong, respectively. Based on these results, we have two observations. Firstly, in scenario 1 with a weak direct link, the passive RIS can indeed achieve a performance improvement, while the active RIS achieves a much higher sum-rate gain. Secondly, in scenario 2 with a strong direct link, the passive RIS achieves only a negligible sum-rate gain, while the active RIS still realizes a noticeable sum-rate gain. For example, when $L = 200$ m, the capacities without RIS, with passive RIS, and with active RIS in scenario 1 are 5.32 bps/Hz, 6.90 bps/Hz, and 31.91 bps/Hz respectively, while in scenario 2, these values are 19.88 bps/Hz, 20.41 bps/Hz, and 33.10 bps/Hz, respectively. For this position, the passive RIS provides a 30% gain in scenario 1 and a negligible 3% gain in scenario 2. By contrast, the active RIS achieves noticeable sum-rate gains of 500% in scenario 1 and 67% in scenario 2, which are much higher than those achieved by the passive RIS in the corresponding scenarios. These results demonstrate that, compared with the existing passive RIS, the proposed active RIS can overcome the “multiplicative fading” effect and achieve noticeable sum-rate gains even when direct link is strong.

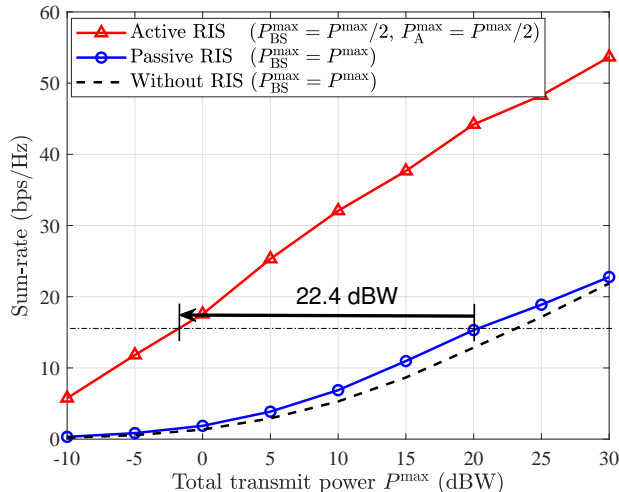
C. The Impact of Key System Parameters on Performance

To gain more insights on active RIS aided communication systems, in this subsection, we study the impact of key parameters, including the total power consumption P^{\max} and the number of RIS elements N , on the sum-rate performance.

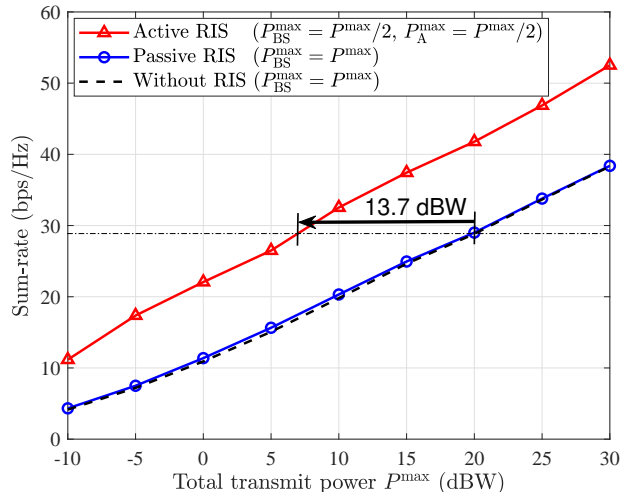
1) *Sum-rate versus total power consumption P^{\max}* : Using the same simulation setup as in Subsection V-B and fixing the distance to $L = 200$ m, we show the users’ sum-rate versus the total power consumption P^{\max} in Fig. 9. For the system with the active RIS, we assume the total power consumption P^{\max} is equally allocated to the BS and the active RIS for

a fair comparison. From Fig. 9 we observe that the passive RIS achieves visible performance gains in scenario 1 where the direct link is weak, while the passive RIS only achieves negligible sum-rate gains in scenario 2 where the direct link is strong. By contrast, in both scenarios, the active RIS realizes a high performance gain. Particularly, we note that, to achieve the same performance as the passive RIS aided system, the required power consumption for the active RIS aided system is much lower. For example, when the total power consumption of the passive RIS aided system is 20 dBW, to achieve the same sum-rate, the active RIS aided system only requires -2.4 dBW in scenario 1 and 6.3 dBW in scenario 2, which correspond to power savings of 22.4 dBW and 13.7 dBW, respectively. The reason for this result is that, for the passive RIS, the total power is only allocated to BS. Thus, all transmit power is affected by the large path loss of the full BS-RIS-user link. However, for the active RIS, half of the transmit power is allocated to the active RIS, and this part of the power is only affected by the path loss of the RIS-user link. This clearly explains why, to achieve the same performance, the total power required by the active RIS aided system is lower than that required by the passive RIS aided system. Thus, the proposed active RIS is promising for reducing the power consumption of communication systems.

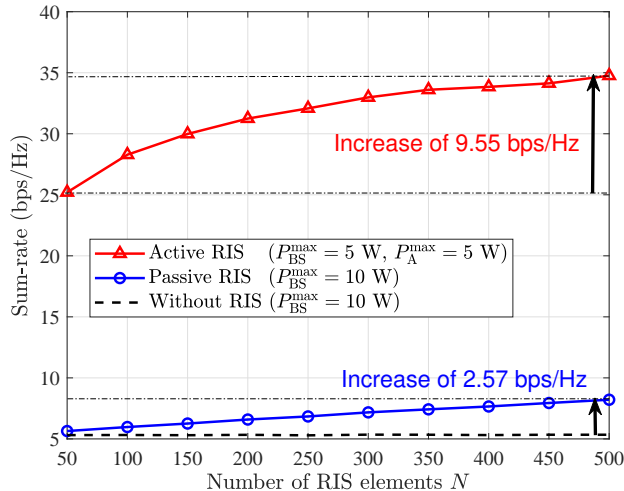
2) *Sum-rate versus number of RIS elements N* : For the same setup as in Fig. 9, we plot the users’ sum-rate versus the number of RIS elements N in Fig. 10. From Fig. 10, we observe that, as the number of RIS elements N increases, both the passive RIS and the active RIS achieve higher sum-rate gains, while the performance improvement for the active RIS aided system is much larger than that for the passive RIS aided system. For example, when N increases from 50 to 500, the sum-rate of the passive RIS aided system increases from 5.64 bps/Hz to 8.21 bps/Hz in scenario 1 (increase of 2.57 bps/Hz) and from 19.76 bps/Hz to 20.54 bps/Hz in scenario 2 (increase of 0.78 bps/Hz), respectively. By contrast, the sum-rate of the active RIS aided system increases from 25.20 bps/Hz to



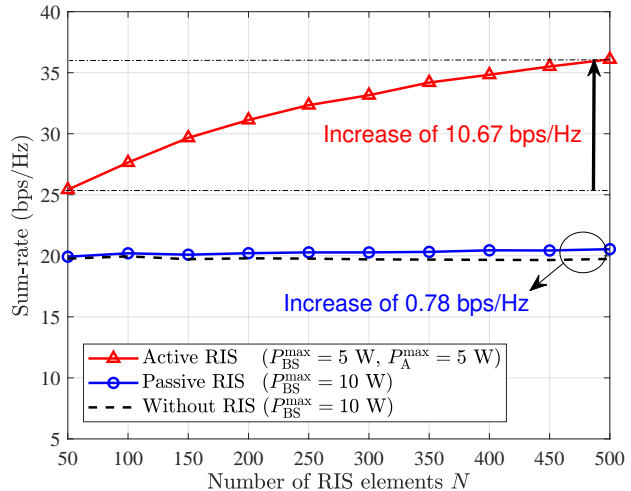
(a) Scenario 1 with a weak direct link.



(b) Scenario 2 with a strong direct link.

Fig. 9. Simulation results for the sum-rate versus total power consumption P^{\max} in an RIS-aided MIMO system.

(a) Scenario 1 with a weak direct link.



(b) Scenario 2 with a strong direct link.

Fig. 10. Simulation results for the sum-rate versus the number of RIS elements N in an RIS-aided MIMO system.

34.75 bps/Hz in scenario 1 (increase of 9.55 bps/Hz) and from 25.42 bps/Hz to 36.09 bps/Hz in scenario 2 (increase of 10.67 bps/Hz), respectively. These results show that the sum-rate increase of the active RIS aided system is much higher than that of the passive RIS aided system. This indicates that, as long as the number of RIS elements N is not exceedingly large (such as millions of elements), compared with the passive RIS, increasing the number of elements of the active RIS is much more efficient for improving the communication performance, which is in agreement with the performance analysis in Section III.

VI. CONCLUSIONS AND FUTURE WORKS

In this paper, we have proposed the concept of active RISs to overcome the fundamental limitation of the “multiplicative fading” effect. Then, we have developed a signal model for

active RISs, which has been validated by a fabricated active RIS element through experimental measurements. Based on the proposed signal model, we have analyzed the asymptotic performance of active RISs and then formulated an optimization problem to maximize the sum-rate in an active RIS aided multi-user MIMO system. Subsequently, we have proposed a joint beamforming and precoding algorithm to solve this problem. Finally, experimental and simulation results have shown that, compared with the benchmark scheme without RIS, the existing passive RIS can realize only a negligible sum-rate gain of about 3% in a typical application scenario, while the proposed active RIS can achieve a substantial sum-rate gain of about 67%, thus indeed overcoming the fundamental limitation of the “multiplicative fading” effect. In the future, many research directions for active RISs are worth pursuing, including hardware design [23], prototype development [7],

channel estimation [21], and energy efficiency analysis [10].

APPENDIX A
PROOF OF LEMMA 2

Since the considered scenario is an active RIS aided SISO system without direct link, for notational simplicity, some matrices and vectors in (4) can be redefined as $\mathbf{G} := \mathbf{g} = [g_1, \dots, g_N]^T$, $\mathbf{f}_k := \mathbf{f} = [f_1, \dots, f_N]^T$, and $\mathbf{w}_k := w$. Thus, the downlink transmission model in (4) can be rewritten as

$$r = \underbrace{p\mathbf{f}^H\Theta\mathbf{g}}_{\text{Reflected link}} ws + \underbrace{p\mathbf{f}^H\Theta\mathbf{v}}_{\text{Noise introduced by active RIS}} + \underbrace{z}_{\text{Noise introduced at user}}, \quad (25)$$

where $r \in \mathbb{C}$ is the signal received by the user. Based on the transmission model in (25), the SNR at the user, γ , the transmit power at the BS, P_{BS} , and the reflect power of the active RIS, P_A , can be respectively derived as follows:

$$\gamma = \frac{|p\mathbf{f}^H\Theta\mathbf{g}w|^2}{p^2\|\mathbf{f}^H\Theta\|^2\sigma_v^2 + \sigma^2} \quad (26a)$$

$$P_{\text{BS}} = |w|^2, \quad (26b)$$

$$P_A = p^2\|\Theta\mathbf{g}w\|^2 + p^2N\sigma_v^2. \quad (26c)$$

Thus, the maximization of the user's SNR γ , subject to the power constraints at the BS and the active RIS, can be formulated as follows:

$$\begin{aligned} \max_{w, p, \Theta} \quad & \gamma = \frac{|p\mathbf{f}^H\Theta\mathbf{g}w|^2}{p^2\|\mathbf{f}^H\Theta\|^2\sigma_v^2 + \sigma^2}, \\ \text{s.t.} \quad & C_1 : |w|^2 \leq P_{\text{BS}}^{\max}, \\ & C_2 : p^2\|\Theta\mathbf{g}w\|^2 + p^2N\sigma_v^2 \leq P_A^{\max}, \end{aligned} \quad (27)$$

where P_{BS}^{\max} and P_A^{\max} denote the maximum transmit power and the maximum reflect power at the BS and the active RIS, respectively. Then, the optimal solution of problem (27) can be obtained by the Lagrange multiplier method as follows:

$$w^{\text{opt}} = \sqrt{P_{\text{BS}}^{\max}}, \quad (28a)$$

$$\theta_n^{\text{opt}} = \angle f_n - \angle g_n, \quad \forall n \in \{1, \dots, N\}, \quad (28b)$$

$$p^{\text{opt}} = \sqrt{\frac{P_A^{\max}}{P_{\text{BS}}^{\max} \sum_{n=1}^N |g_n|^2 + N\sigma_v^2}}. \quad (28c)$$

By substituting (28) into (27), the user's maximum achievable SNR for active RISs can be obtained as

$$\gamma_{\text{active}} = \frac{P_{\text{BS}}^{\max} P_A^{\max} \left| \sum_{n=1}^N |f_n| |g_n| \right|^2}{P_A^{\max} \sigma_v^2 \sum_{n=1}^N |f_n|^2 + \sigma^2 \left(P_{\text{BS}}^{\max} \sum_{n=1}^N |g_n|^2 + N\sigma_v^2 \right)}. \quad (29)$$

Note that we assume $\mathbf{f} \sim \mathcal{CN}(\mathbf{0}_N, \varrho_f^2 \mathbf{I}_N)$ and $\mathbf{g} \sim \mathcal{CN}(\mathbf{0}_N, \varrho_g^2 \mathbf{I}_N)$. Thus, by letting $N \rightarrow \infty$ in (29), according to the law of large numbers, we have

$$\sum_{n=1}^N |f_n| |g_n| \rightarrow N \frac{\pi \varrho_f \varrho_g}{4}, \quad (30a)$$

$$\sum_{n=1}^N |g_n|^2 \rightarrow N \varrho_g^2, \quad (30b)$$

$$\sum_{n=1}^N |f_n|^2 \rightarrow N \varrho_f^2. \quad (30c)$$

After substituting (30) into (29), we obtain for the asymptotic SNR for active RISs the expression in (6), which completes the proof.

APPENDIX B
PROOF OF LEMMA 3

According to the related analysis in [33] and Appendix A, the user's achievable SNR for an SISO system aided by a passive RIS and that aided by an active RIS can be respectively written as follows

$$\gamma_{\text{passive}} = \frac{P_{\text{BS-P}}^{\max} \left| \sum_{n=1}^N |f_n| |g_n| \right|^2}{\sigma^2}, \quad (31a)$$

$$\gamma_{\text{active}} = \frac{P_{\text{BS-A}}^{\max} P_A^{\max} \left| \sum_{n=1}^N |f_n| |g_n| \right|^2}{P_A^{\max} \sigma_v^2 \sum_{n=1}^N |f_n|^2 + \sigma^2 \left(P_{\text{BS-A}}^{\max} \sum_{n=1}^N |g_n|^2 + N\sigma_v^2 \right)}, \quad (31b)$$

where $P_{\text{BS-A}}^{\max}$ denotes the maximum BS transmit power for the active RIS aided system and $P_{\text{BS-P}}^{\max}$ denotes that for the passive RIS aided system. By solving $\gamma_{\text{passive}} \geq \gamma_{\text{active}}$ according to (31), we have

$$\begin{aligned} N &\geq \\ &\frac{P_{\text{BS-A}}^{\max}}{P_{\text{BS-P}}^{\max}} \frac{P_A^{\max} \sigma^2}{P_A^{\max} \sigma_v^2 \frac{1}{N} \sum_{n=1}^N |f_n|^2 + \sigma^2 \left(P_{\text{BS}}^{\max} \frac{1}{N} \sum_{n=1}^N |g_n|^2 + \sigma_v^2 \right)} \\ &\approx \frac{P_{\text{BS-A}}^{\max}}{P_{\text{BS-P}}^{\max}} \frac{P_A^{\max} \sigma^2}{\left(P_A^{\max} \sigma_v^2 \varrho_f^2 + P_{\text{BS-A}}^{\max} \sigma^2 \varrho_g^2 + \sigma^2 \sigma_v^2 \right)}, \end{aligned} \quad (32)$$

where we assume again that $\mathbf{f} \sim \mathcal{CN}(\mathbf{0}_N, \varrho_f^2 \mathbf{I}_N)$ and $\mathbf{g} \sim \mathcal{CN}(\mathbf{0}_N, \varrho_g^2 \mathbf{I}_N)$. Since the number of RIS elements N is usually large, the components $\frac{1}{N} \sum_{n=1}^N |f_n|^2$ and $\frac{1}{N} \sum_{n=1}^N |g_n|^2$ in (32) were approximated by ϱ_f^2 and ϱ_g^2 . This completes the proof.

APPENDIX C
PROOF OF LEMMA 4

After merging \mathbf{P} and Θ as $\Psi = \mathbf{P}\Theta = \text{diag}(p_1 e^{j\theta_1}, \dots, p_N e^{j\theta_N}) \in \mathbb{C}^{N \times N}$, the original problem \mathcal{P}_o in (10) can be equivalently rewritten as follows:

$$\begin{aligned} \mathcal{P}' : \quad & \max_{\mathbf{w}, \Psi} R_{\text{sum}}(\mathbf{w}, \Psi) = \sum_{k=1}^K \log_2(1 + \gamma_k), \\ \text{s.t.} \quad & C_1 : \sum_{k=1}^K \|\mathbf{w}_k\|^2 \leq P_{\text{BS}}^{\max}, \\ & C_2 : \sum_{k=1}^K \|\Psi \mathbf{G} \mathbf{w}_k\|^2 + \|\Psi\|^2 \sigma_v^2 \leq P_A^{\max}. \end{aligned} \quad (33)$$

To tackle the non-convex sum-of-logarithms in the original problem \mathcal{P}_o in (10), we apply the Lagrangian dual transform proposed in [35] to decompose the sum-rate objective R_{sum} . By introducing an auxiliary variable to be optimized, $\rho :=$

$[\rho_1, \dots, \rho_K] \in \mathbb{R}_+^K$, the sum-rate objective R_{sum} in \mathcal{P}' in (33) can be equivalently replaced by

$$\begin{aligned} R'_{\text{sum}}(\mathbf{w}, \Psi, \rho) &= \sum_{k=1}^K \ln(1 + \rho_k) - \sum_{k=1}^K \rho_k + \sum_{k=1}^K \frac{(1 + \rho_k) \gamma_k}{1 + \gamma_k} \\ &= \sum_{k=1}^K \ln(1 + \rho_k) - \sum_{k=1}^K \rho_k + \sum_{k=1}^K g'(\mathbf{w}, \Psi, \rho_k), \end{aligned} \quad (34)$$

where function $g'(\mathbf{w}, \Psi, \rho_k)$ is defined as follows

$$g'(\mathbf{w}, \Psi, \rho_k) = \frac{(1 + \rho_k) |\bar{\mathbf{h}}_k^H \mathbf{w}_k|^2}{\sum_{j=1}^K |\bar{\mathbf{h}}_k^H \mathbf{w}_j|^2 + \|\mathbf{f}_k^H \Psi\|^2 \sigma_v^2 + \sigma^2}. \quad (35)$$

For any given \mathbf{w} and Ψ , it can be proved by solving $\frac{\partial R'_{\text{sum}}}{\partial \rho} = 0$ that

$$\max_{\rho} \{R'_{\text{sum}}(\mathbf{w}, \Psi, \rho)\} = \frac{1}{\log_2 e} R_{\text{sum}}(\mathbf{w}, \Psi). \quad (36)$$

This means that the optimal solution to problem \mathcal{P}' in (33) remains unchanged after R_{sum} is replaced by R'_{sum} . However, due to the non-convex fraction g' in (35), the problem is still difficult to solve.

To tackle this problem, we further apply the quadratic transform proposed in [35] to decouple fraction g' in (35). By introducing one more auxiliary variable to be also optimized, $\varpi := [\varpi_1, \dots, \varpi_K] \in \mathbb{C}^K$, fraction g' in (35) can be equivalently replaced by

$$\begin{aligned} g(\mathbf{w}, \Psi, \rho_k, \varpi_k) &= 2\sqrt{(1 + \rho_k)} \Re \{ \varpi_k^* \bar{\mathbf{h}}_k^H \mathbf{w}_k \} - \\ &|\varpi_k|^2 \left(\sum_{j=1}^K |\bar{\mathbf{h}}_k^H \mathbf{w}_j|^2 + \|\mathbf{f}_k^H \Psi\|^2 \sigma_v^2 + \sigma^2 \right). \end{aligned} \quad (37)$$

For any given \mathbf{w} , Ψ , and ρ_k , it can be proved by solving $\frac{\partial g}{\partial \varpi_k} = 0$ that

$$\max_{\varpi_k} \{g(\mathbf{w}, \Psi, \rho_k, \varpi_k)\} = g'(\mathbf{w}, \Psi, \rho_k), \quad (38)$$

which means that the introduction of auxiliary variable ϖ will not influence the optimal solution of problem \mathcal{P}' in (33).

Therefore, by combing (33), (34), and (37), the original problem \mathcal{P}_o in (10) can be equivalently reformulated as follows

$$\begin{aligned} \mathcal{P}_1 : \quad \max_{\mathbf{w}, \Psi, \rho, \varpi} R'_{\text{sum}}(\mathbf{w}, \Psi, \rho, \varpi) &= \sum_{k=1}^K \ln(1 + \rho_k) \\ &- \sum_{k=1}^K \rho_k + \sum_{k=1}^K g(\mathbf{w}, \Psi, \rho_k, \varpi_k), \end{aligned} \quad (39)$$

s.t. $C_1, C_2,$

where $\max_{\rho, \varpi} \{R'_{\text{sum}}(\mathbf{w}, \Psi, \rho, \varpi)\} = \frac{1}{\log_2 e} R_{\text{sum}}(\mathbf{w}, \Psi)$ holds. This completes the proof.

REFERENCES

- [1] L. Zhang, X. Q. Chen, S. Liu, Q. Zhang, J. Zhao, J. Y. Dai, G. D. Bai, X. Wan, Q. Cheng, G. Castaldi, V. Galdi, and T. J. Cui, "Space-time-coding digital metasurfaces," *Nat. Commun.*, vol. 9, no. 4338, Oct. 2018.
- [2] X. Ni, A. V. Kildishev, and V. M. Shalaev, "Metasurface holograms for visible light," *Nat. Commun.*, vol. 4, no. 2807, Nov. 2013.
- [3] H. Ren, "A light-programmable metasurface," *Nat. Elect.*, vol. 3, pp. 137–138, Mar. 2020.
- [4] S. Venkatesh, X. Lu, H. Saeidi, and K. Sengupta, "A high-speed programmable and scalable terahertz holographic metasurface based on tiled CMOS chips," *Nat. Elect.*, vol. 3, pp. 785–793, Dec. 2020.
- [5] M. Di Renzo, A. Zappone, M. Debbah, M. S. Alouini, C. Yuen, J. de Rosny, and S. Tretyakov, "Smart radio environments empowered by reconfigurable intelligent surfaces: How it works, state of research, and the road ahead," *IEEE J. Sel. Areas Commun.*, vol. 38, no. 11, pp. 2450–2525, Nov. 2020.
- [6] E. Basar, M. Di Renzo, J. De Rosny, M. Debbah, M. Alouini, and R. Zhang, "Wireless communications through reconfigurable intelligent surfaces," *IEEE Access*, vol. 7, pp. 116753–116773, Aug. 2019.
- [7] L. Dai, B. Wang, M. Wang, X. Yang, J. Tan, S. Bi, S. Xu, F. Yang, Z. Chen, M. Di Renzo, C. B. Chae, and L. Hanzo, "Reconfigurable intelligent surface-based wireless communications: Antenna design, prototyping, and experimental results," *IEEE Access*, vol. 8, pp. 45913–45923, Mar. 2020.
- [8] C. Huang, R. Mo, and C. Yuen, "Reconfigurable intelligent surface assisted multiuser MISO systems exploiting deep reinforcement learning," *IEEE J. Sel. Areas Commun.*, vol. 38, no. 8, pp. 1839–1850, Aug. 2020.
- [9] P. Wang, J. Fang, X. Yuan, Z. Chen, and H. Li, "Intelligent reflecting surface-assisted millimeter wave communications: Joint active and passive precoding design," *IEEE Trans. Veh. Technol.*, vol. 69, no. 12, pp. 14960–14973, Dec. 2020.
- [10] C. Huang, A. Zappone, G. C. Alexandropoulos, M. Debbah, and C. Yuen, "Reconfigurable intelligent surfaces for energy efficiency in wireless communication," *IEEE Trans. Wireless Commun.*, vol. 18, no. 8, pp. 4157–4170, Aug. 2019.
- [11] H. Zhao, Y. Shuang, M. Wei, T. J. Cui, P. Hougue, and L. Li, "Metasurface-assisted massive backscatter wireless communication with commodity Wi-Fi signals," *Nat. Commun.*, vol. 11, no. 3926, Aug. 2020.
- [12] M. Faraji-Dana, E. Arbabi, A. Arbabi, S. M. Kamali, H. Kwon, and A. Faraon, "Compact folded metasurface spectrometer," *Nat. Commun.*, vol. 9, no. 4196, Oct. 2013.
- [13] J. Park, B. G. Jeong, S. I. Kim, D. Lee, J. Kim, C. Shin, C. B. Lee, T. Otsuka, J. Kyoung, S. Kim, K. Yang, Y. Park, J. Lee, I. Hwang, J. Jang, S. H. Song, M. L. Brongersma, K. Ha, S. Hwang, H. Choo, and B. L. Choi, "All-solid-state spatial light modulator with independent phase and amplitude control for three-dimensional LiDAR applications," *Nat. Nanotechnol.*, vol. 16, p. 69–76, Oct. 2020.
- [14] T. L. Marzetta, "Noncooperative cellular wireless with unlimited numbers of base station antennas," *IEEE Trans. Wireless Commun.*, vol. 9, no. 11, pp. 3590–3600, Nov. 2010.
- [15] W. Zhao, G. Wang, S. Atapattu, T. A. Tsiftsis, and C. Tellambura, "Is backscatter link stronger than direct link in reconfigurable intelligent surface-assisted system?" *IEEE Commun. Lett.*, vol. 24, no. 6, pp. 1342–1346, Jun. 2020.
- [16] T. Hou, Y. Liu, Z. Song, X. Sun, and Y. Chen, "MIMO-NOMA networks relying on reconfigurable intelligent surface: A signal cancellation-based design," *IEEE Trans. Commun.*, vol. 68, no. 11, pp. 6932–6944, Nov. 2020.
- [17] Z. Zhang and L. Dai, "A joint precoding framework for wideband reconfigurable intelligent surface-aided cell-free network," *IEEE Trans. Signal Process.*, vol. 69, pp. 4085–4101, Aug. 2021.
- [18] M. Najafi, V. Jamali, R. Schober, and H. V. Poor, "Physics-based modeling and scalable optimization of large intelligent reflecting surfaces," *IEEE Trans. Commun.*, vol. 69, no. 4, pp. 2673–2691, Apr. 2021.
- [19] H. Yang, F. Yang, X. Cao, S. Xu, J. Gao, X. Chen, M. Li, and T. Li, "A 1600-element dual-frequency electronically reconfigurable reflectarray at X/Ku-band," *IEEE Trans. Antennas Propag.*, vol. 65, no. 6, pp. 3024–3032, Jun. 2017.
- [20] D. Headland, T. Niu, E. Carrasco, D. Abbott, S. Sriram, M. Bhaskaran, C. Fumeaux, and W. Withayachumnankul, "Terahertz reflectarrays and nonuniform metasurfaces," *IEEE J. Sel. Topics Quantum Electron.*, vol. 23, no. 4, pp. 1–18, Aug. 2017.
- [21] C. Hu, L. Dai, S. Han, and X. Wang, "Two-timescale channel estimation for reconfigurable intelligent surface aided wireless communications," *IEEE Trans. Commun.*, vol. 69, no. 11, pp. 7736–7747, Nov. 2021.
- [22] C. Pan, H. Ren, K. Wang, W. Xu, M. Elkashlan, A. Nallanathan, and L. Hanzo, "Multicell MIMO communications relying on intelligent reflecting surfaces," *IEEE Trans. Wireless Commun.*, vol. 19, no. 8, pp. 5218–5233, Aug. 2020.
- [23] J. Lončar, Z. Šipuš, and S. Hrabar, "Ultrathin active polarization-selective metasurface at X-band frequencies," *Physical Review B*, vol. 100, no. 7, p. 075131, Oct. 2019.

- [24] J. Bousquet, S. Magierowski, and G. G. Messier, "A 4-GHz active scatterer in 130-nm CMOS for phase sweep amplify-and-forward," *IEEE Trans. Circuits Syst. I*, vol. 59, no. 3, pp. 529–540, Mar. 2012.
- [25] K. K. Kishor and S. V. Hum, "An amplifying reconfigurable reflectarray antenna," *IEEE Trans. Antennas Propag.*, vol. 60, no. 1, pp. 197–205, Jan. 2012.
- [26] X. Mu, Y. Liu, L. Guo, J. Lin, and R. Schober, "Simultaneously transmitting and reflecting (STAR) RIS aided wireless communications," *IEEE Trans. Wireless Commun.*, Oct. 2021.
- [27] Y. Liu, X. Mu, J. Xu, R. Schober, Y. Hao, H. V. Poor, and L. Hanzo, "STAR: Simultaneous transmission and reflection for 360° coverage by intelligent surfaces," *IEEE Wireless Commun.*, vol. 28, no. 6, pp. 102–109, Dec. 2021.
- [28] S. Zeng, H. Zhang, B. Di, Y. Tan, Z. Han, H. V. Poor, and L. Song, "Reconfigurable intelligent surfaces in 6G: Reflective, transmissive, or both?" *IEEE Commun. Lett.*, vol. 25, no. 6, pp. 2063–2067, Jun. 2021.
- [29] J. He, N. T. Nguyen, R. Schroeder, V. Tapio, J. Kokkonen, and M. Juntti, "Channel estimation and hybrid architectures for ris-assisted communications," in *Proc. 2021 Joint European Conf. Netw. Commun. 6G Summit (EuCNC/6G Summit'21)*, Jun. 2021, pp. 60–65.
- [30] N. T. Nguyen, Q.-D. Vu, K. Lee, and M. Juntti, "Hybrid relay-reflecting intelligent surface-assisted wireless communication," *arXiv preprint arXiv:2103.03900*, Mar. 2021.
- [31] E. Basar, "Transmission through large intelligent surfaces: A new frontier in wireless communications," in *Proc. European Conf. Netw. Commun. (EuCNC'19)*, Jun. 2019, pp. 1–6.
- [32] K. Ntontin, J. Song, and M. D. Renzo, "Multi-antenna relaying and reconfigurable intelligent surfaces: End-to-end SNR and achievable rate," *arXiv preprint arXiv:1908.07967*, Aug. 2019.
- [33] Q. Wu and R. Zhang, "Intelligent reflecting surface enhanced wireless network via joint active and passive beamforming," *IEEE Trans. Wireless Commun.*, vol. 18, no. 11, pp. 5394–5409, Nov. 2019.
- [34] T. Marzetta and B. Hochwald, "Capacity of a mobile multiple-antenna communication link in Rayleigh flat fading," *IEEE Trans. Inf. Theory*, vol. 45, no. 1, pp. 139–157, Jan. 1999.
- [35] K. Shen and W. Yu, "Fractional programming for communication systems—part I: Power control and beamforming," *IEEE Trans. Signal Process.*, vol. 66, no. 10, pp. 2616–2630, May 2018.
- [36] S. Boyd, N. Parikh, E. Chu, B. Peleato, and J. Eckstein, "Distributed optimization and statistical learning via the alternating direction method of multipliers," Nov. 2014, [Online] Available: https://stanford.edu/~boyd/papers/pdf/admm_distr_stats.pdf.
- [37] M. Grant and S. Boyd, "CVX: Matlab software for disciplined convex programming, version 2.1, [Online] Available: <http://cvxr.com/cvx>," Mar. 2014.
- [38] X. Chen and F. Yang, "Nonlinear electromagnetic surfaces: Theory, design and application," *Master Thesis in Tsinghua University*, May 2020, [Online] Available: <http://etds.lib.tsinghua.edu.cn/Thesis>.
- [39] "Further advancements for E-UTRA physical layer aspects (release 9)," *3GPP TS 36.814*, Mar. 2010.
- [40] H. Guo, Y. Liang, J. Chen, and E. G. Larsson, "Weighted sum-rate maximization for reconfigurable intelligent surface aided wireless networks," *IEEE Trans. Wireless Commun.*, vol. 19, no. 5, pp. 3064–3076, May 2020.